Performance of a 6 × 6 mm^2 SiPM Module for Time-Domain Diffuse Optics

Anurag Behera, Fabio Acerbi, *Member, IEEE*, Alberto Gola, Alberto Dalla Mora, and Laura Di Sieno

***Abstract*—In this work we present a detector module based on large-area silicon photomultiplier, whose design has been optimized for time-domain diffuse optics measurements. In this application, to the best of our knowledge, it represents the largest area detector ever demonstrated, with expected breakthrough performance in terms of scattered light harvesting efficiency. It has been characterized using widely adopted protocols for performance assessment of instruments. We demonstrate the superior light harvesting capability and improved depth sensitivity, which can reach 4 cm. Moreover, the retrieval of optical properties has been demonstrated to be linear and with sufficient accuracy in the range corresponding to the human tissues. As a first step toward clinical application, we first performed *in-vivo* measurement at very large source-detector distances to show the suitability of the realized detector to tackle new challenges like lung or heart optical monitoring as well as imaging of deep cerebral function.**

***Index Terms*—Optical imaging, photon counting, silicon photomultiplier, single-photon detector, time-correlated single-photon counting, time-domain diffuse optics.**

I. Introduction

TIME DOMAIN diffuse optics (TD-DO) is an optical non-invasive technique which relies on the injection of fast laser pulses (ps duration) into the medium to be investigated [1]. After the propagation of photons in the sample (due to both scattering and absorption events) some of them are re-emitted from the medium and can be detected at a given distance from the source. The distance between injection and collection point is called source-detector separation (ρ). The main advantages of the TD-DO technique with respect to the Continuous Wave (CW) one are: i) the capability to disentangle the reduced scattering coefficient (μ_s') from the absorption one (μ_a) with a single source-detector pair; ii) the encoding of the mean penetration depth reached by photons in their arrival time. Thanks to this higher information content, TD-DO is gaining interests within scientists even though the CW technique relies on smaller and less expensive equipment, thus being more diffused in clinical and consumer devices [2].

However, in the last years, few groups worked on the miniaturization of the main components of the TD-DO systems (such as laser and timing electronics) to reduce the cost and the dimensions of the setups [2]. On the other hand, there is the trend to improve the setup performances trying to reach the limits of the TD-DO. Such an achievement requires improvements of the TD-DO setups on two different sides: i) the light harvesting capability of the detector and ii) the high-throughput of the timing electronics. For the former aspect, TD-DO recently adopted the Silicon PhotoMultipliers (SiPMs) as detector, thus increasing the light harvesting capability thanks to the large active area and the improved numerical aperture due to the direct contact between the sample and the detector itself [3]. To fulfill both conditions, traditional detectors (such as PhotoMultiplier Tubes or hybrid detectors) cannot be profitably used, as discussed in Ref. [2]. Additionally, SiPMs have all the advantages of solid-state detectors (such as low biasing voltage, ruggedness and higher insensitivity to magnetic field), thus being considered as a promising alternative to standard detectors for TD-DO. Starting from the first works in 2015, the use of SiPMs have been demonstrated in several TD-DO applications (such as spectroscopy, tomography and brain imaging [3], [4]) and a trend towards large area and probe-hosted devices has been reported in several works ([3], [5], [6]).

On the other hand, also timing electronics were improved to sustain an increased count-rate. Indeed, new generation of integrated time-to-digital converters (TDCs) working at sustained count-rates of up to Gcps have been published in the last few years, while some stand-alone TDC are commercially available [7]–[12].

In a previous paper by some of us, the use of large-area SiPM (actual sensitive area: 7.38 mm^2) coupled to a high throughput timing electronics has been studied for TD-DO applications demonstrating the possibility of working with large-area SiPM characterized by a broad temporal response [5]. However, the achievable performances were limited mainly for two reasons: i) the high dark count rate (DCR, caused by the absence of thermal cooling) and ii) its sensitivity to electromagnetic disturbances that determines fluctuations of the background voltage.

Additionally, to reach the theoretical limits an even larger active area is required. Indeed, the improvement in the sensitive area of the detector (i.e., in its light harvesting capability) will open the way to unexplored yet interesting challenges for

Manuscript received April 1, 2021; accepted September 30, 2021. Date of publication October 6, 2021; date of current version December 6, 2021. This work was supported in part by the ATTRACT project funded by the EU under Grant Agreement 777222, and in part by European Commission under H2020 framework with the BITMAP under Project 675332. *(Corresponding author: Laura Di Sieno)*

Anurag Behera, Alberto Dalla Mora, and Laura Di Sieno are with the Politecnico di Milano, Dipartimento di Fisica, Milano 20133, Italy (e-mail: anurag.behera@polimi.it; alberto.dallamora@polimi.it; laura.disieno@polimi.it).

Fabio Acerbi and Alberto Gola are with Fondazione Bruno Kessler (FBK), Trento 38123, Italy (e-mail: acerbi@fbk.eu; gola@fbk.eu).

Color versions of one or more figures in this article are available at https://doi.org/10.1109/JSTQE.2021.3117880.

Digital Object Identifier 10.1109/JSTQE.2021.3117880

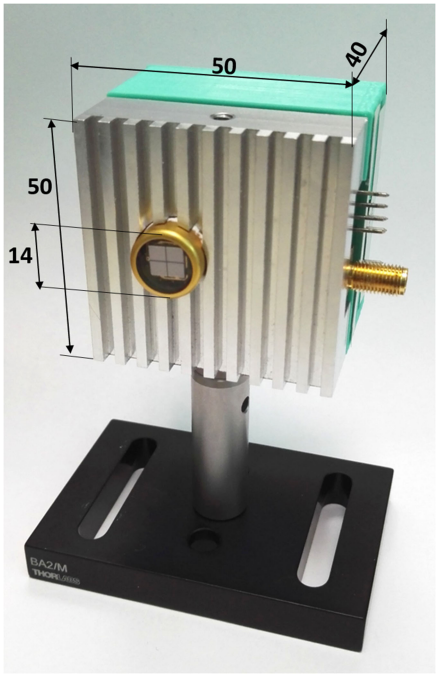

Fig. 1. Picture of the large area SiPM with its case that contains the associated front-end electronics. The dimensions are expressed in mm.

TD-DO such as, the measurement of human head and chest in transmittance geometry.

To this end, in the framework of the "SP-LADOS" project (funded by the European Commission through the Attract project), a new SiPM detector featuring a larger sensitive area (32.1 mm^2) and a relatively low DCR was developed.

In this paper, we validate the realized detector making use of figures of merit defined in shared protocols for the assessment of basic hardware performances of DO components/system (i.e., BIP protocol [13]) as well as performances of the system in retrieving optical properties in homogeneous medium and in the capability to detect, localize, and quantify absorption changes (i.e., MEDPHOT and nEUROPt protocols, respectively [14], [15]). Additionally, some preliminary *in-vivo* measurements to show the capability of the system to measure different organs/regions of the human body are shown.

The manuscript is divided as follows: Section II deals the setup used (with a particular focus on the detector) and with data analysis methods; Section III describes and discusses the results, while Section IV draws conclusions and future perspectives of the work.

II. Materials and Methods

A. Detector Module Description

Fig. 1 shows a picture of the custom-made detector module with its dimensions. It is based on a large area SiPM of nominally 6×6 (36 mm^2) active area, which is made by 4 different SiPM chips (each one with dimension of about 3×3 mm^2, with 35 μm cell pitch) placed side by side, with common back contact and all in parallel. These SiPMs are designed and fabricated in FBK (Trento, Italy). The cell fill factor for the single SiPM is > 80%. Considering the chips borders the overall effective active area of the sensor is about 32.1 mm^2. The SiPMs are based on the Vacuum UltraViolet, High Density of cells (VUV-HD) low-field technology which has been chosen because of the low primary noise (DCR) and correlated noise that can be achieved, as well as the higher reduction of noise achievable reducing the temperature, thanks to the lower electric field value [16–18]. The SiPMs are Peltier cooled (2 stage thermoelectric cooler -TEC-) at about -15°C, inside a vacuum-sealed TO8 package. The module also contains a custom-made front-end circuit (with a two stage signal amplifier) and the temperature controller. The first stage amplifier is based on trans-impedance configuration. The total trans-impedance gain is about 10000 V/A. The custom TEC controller has been designed and optimized to reduce any possible voltage interference on the SiPM signal, which is very important in precise timing application like the one proposed here. The module is relatively compact, being 5×5×4 cm^3. The front part is made with aluminum heat-sink, CNC (Computerized Numerical Control) manufactured, whereas the back is 3D plastic printed.

The SiPMs have been pre-characterized in FBK on wafer level and then functionally tested when mounted in the module, using the methodology described in [16]. The DCR is around 80 kcps/mm^2 (kilocounts per second per 1 mm^2 active area) at 20°C, with 38 V bias, i.e., 5.8 V excess bias. At the same bias, the afterpulsing probability (measured as in [16]) is in the order of a few percent [19]. More details on the module electronic design and characterization can be found in Ref. [20]

B. Setup and Measurements Description

To ensure performance in line with state-of-the-art devices, this detector was characterized under internationally accepted protocols for performance assessment of diffuse optics instrument namely BIP, MEDPHOT and nEUROPt [13–15]. The experimental set up, the methods and the data analysis used for each protocol are discussed in the following sections.

1) BIP Protocol: BIP (which stands for Basic Instrumental Performance protocol [13]), aims at characterizing system without the sample. Relevant parameters such as diffuse responsivity of the detector (i.e., light harvesting capability, henceforth indicated simply as responsivity), temporal Instrument Response Function (IRF), its background noise and stability over time are evaluated.

Fig. 2 shows the schematic of the experimental set up used for the measurements. A SuperK EXTREME, (NKT Photonics, Denmark) supercontinuum laser operating at a repetition rate of 40 MHz was used to provide laser pulses over a broad range of wavelengths (in this work: 600-1000 nm) selected with the help of a computer controlled rotating prism. The output light intensity was regulated using a circular variable neutral density filter, mounted on a u-bench. The attenuated light was incident on the sample and the signal was collected by the detector placed in-contact in transmittance geometry. The placement of the detector was adjusted to ensure that its geometrical center was aligned with respect to the injection fiber. The power supply for the

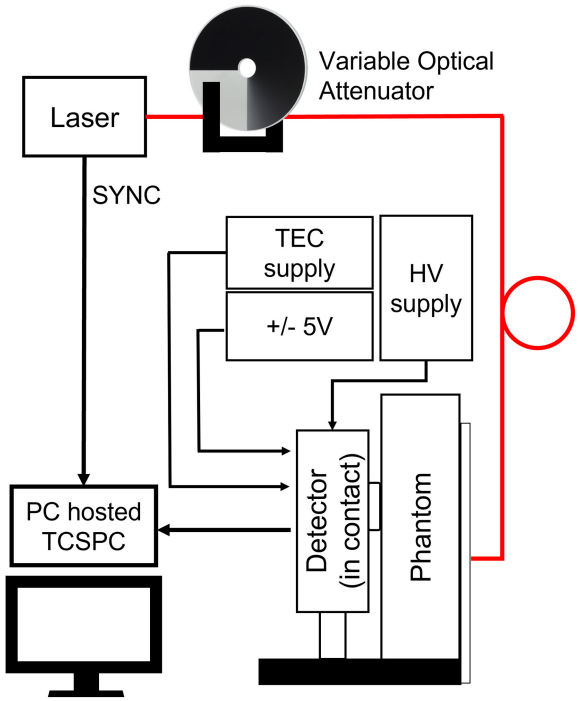

Fig. 2. Schematic of the experimental setup.

module, which included i) detector biasing high voltage (HV), ii) TEC power supply, and iii) $\pm$ 5 V for the front-end amplifier, were provided using commercially available power supply units. A PC hosted TCSPC board (SPC-130, Becker & Hickl GmbH, Germany) was used to build the histograms of distribution of time-of-flight (DTOF).

As regards to the tests, the responsivity describes the detector overall diffuse photon collection efficiency and it is impacted by detector active area, its numerical aperture (NA), fill factor as well as its quantum efficiency at the measured wavelength. Simply put, responsivity is the ratio of the measured signal to the injected photon radiance. A calibrated solid slab of known photon transmittance factor is used to link the injected laser power to wavelength dependent photon radiance. Responsivity was measured from 600 nm to 1000 nm in steps of 25 nm. For each wavelength, 10 acquisitions of 1 s each were acquired along with the output laser power at that wavelength. Using the wavelength dependent photon transmittance factor for the phantom, the spectral responsivity was calculated as dictated in [13].

Unlike responsivity that depends on the detection chain alone, temporal IRF depends on injected laser pulse shape, the response of the detector and the broadening due to the dispersion of the fiber-optics and all non-idealities of the optical setup. Any model-based reconstruction of tissue optical properties requires an accurate knowledge of an IRF that duplicates the conditions of the measurement. To acquire this measurement, a thin Teflon layer is placed between the source fiber and the detector to distribute the injected intensity uniformly over the entire active area and numerical aperture of the detector without introducing additional broadening. Key features of the IRF are its full-width at half-maximum (FWHM) and its background value. The FWHM gives information on the overall timing resolution of the system, while the background limits the achievable dynamic range. The stability of the IRF over time was monitored as it is crucial in determining the suitability of the system in monitoring and retrieving over time small externally induced changes. This was done over a 10-hour period (with one curve of 10 second acquisition time recorded every 10 minutes). The stability in terms of overall number of counts, background noise, FWHM of the IRF and its temporal position (i.e., barycenter) were evaluated.

Moreover, the background noise floor of the detector was computed. It comprises of signal-independent and a signal-dependent sources: the dark-count of the detector and its afterpulsing respectively. The DCR of the detector is measured by acquiring 10 acquisitions of 1 second each, without any light source. The afterpulsing noise is calculated by subtracting the DCR of the detector from the overall background noise floor taken as the part of the IRF where the signal is not present. As dictated in [13] afterpulsing ratio is calculated by normalizing the correlated noise with the overall counts in the IRF and is given by:

$$R_{AP} = \frac{N_{\mathrm{mean},bkg} - N_{\mathrm{mean,dark}}}{N_{\mathrm{tot},IRF}} \frac{T_{\mathrm{laser}}}{\Delta T} \tag{1}$$

where $N_{\mathrm{mean,bkg}}$ and $N_{\mathrm{mean,dark}}$ represent the mean background counts and the dark-counts respectively, $N_{\mathrm{tot,IRF}}$ represents the total counts of the IRF with the background subtracted, while T_{laser} and ΔT are the period of the laser pulses and the time-bin of the TCSPC board. The afterpulsing ratio was computed over the entire spectral range.

2) MEDPHOT Protocol: MEDPHOT protocol [14] evaluates the system's ability to reliably measure optical properties of homogeneous media. A set of 32 homogeneous solid phantoms based on epoxy resin with TiO_2 and black toner powders were used ([14], [21]). Their concentrations are tailored to span a wide range of absorption (8 nominal values from 0 to 0.35 cm^{-1} in steps of 0.05 cm-^{1} measured at 800 nm, named from 1 to 8) and reduced scattering coefficients (4 nominal values from 0 to 20 cm^{-1} in steps of 5 cm^{-1} at 800 nm named from A to D). All the measurements were performed in transmittance geometry (thickness of the phantom of 4.01 $\pm$ 0.06 cm).

The experimental setup used for the MEDPHOT protocol was similar to that shown in Fig. 2 with the distinction of the laser. The supercontinuum laser (average output power: 1 mW) was replaced by a more powerful (up to 50 mW) diode laser with emission peak at 670 nm (LDH-P-670) driven at a repetition rate of 40 MHz using a commercial laser driver (PDL 828 "Sepia II",Picoquant GmbH, Germany), that also provided the sync signal to the PC hosted TCSPC board. The maximum power on the sample was around 7 mW.

For each phantom, 60 acquisitions of 1 second each were taken. To improve the overall signal-to-noise ratio, groups of 3 curves were summed to obtain a total of 20 curves (each one with an equivalent integration time of 3 s). To recover the optical properties a fitting procedure (as described in [22], [23]) based on analytical solution of radiative transport equation under the diffusion approximation in transmittance geometry

for a homogeneous slab using partial current boundary conditions [24] was employed. To take into account non-idealities of the system, the theoretical homogenous curve generated by the model was convolved with the experimentally obtained IRF. Using a Levenberg-Marquardt minimization procedure, the model-based curves were fitted to the experimentally obtained ones to retrieve μ_{a} and $\mu_{\mathrm{s}}^{'}$.

The retrieved optical properties were used to evaluate the ability of the system in following linear changes in μ_{a} and $\mu_{\mathrm{s}}^{'}$, as well as the dependence of retrieving μ_{a} on $\mu_{\mathrm{s}}^{'}$ and vice versa.

For each phantom, the average value of the optical properties as well as the standard deviation over the 20 repetitions were computed.

3) nEUROPt Protocol: The nEUROPt protocol [15] evaluates the ability of the system in detecting, localizing and quantifying local absorption changes within a homogeneous background. To mimic the presence of an absorption perturbation, a totally absorbing inclusion was used [25], [26]. A black cylinder (made of black polyvinyl chloride) of volume 100 mm^3, which corresponds to an absorption change ($\Delta\mu_a$) of 0.17 cm^{-1} over a volume of 1000 mm^3 [25] was used as an absorption inhomogeneity within a homogeneous liquid phantom composed of a given proportion of intralipid, water and ink to have the desired optical properties ($\mu_a = 0.1$ cm^{-1} and $\mu_s' = 10$ cm^{-1}) [27]. The inclusion was translated in depth, with the distance from the liquid surface to the center of the inclusion measured as z (i.e., the depth of the perturbation). The optical setup is the same used for MEDPHOT protocol and described in Sect. II.B.2). The reflectance curves were acquired for different inclusion depths ranging from 0 mm to 50 mm in steps of 2 mm, with z = 60 mm corresponding to the homogeneous condition (i.e., where the effect of the perturbation is negligible). For each position, 10 acquisitions of 1 s each were acquired. This procedure was repeated for different source-detector separations (ρ): i) a commonly used standard condition ($\rho = 3$ cm); ii) uncommon large distances allowed by the high detector sensitivity ($\rho = 6$, 7, 8, 9 and 10 cm).

For each source-detector separation, contrast and Contrast-to-Noise Ratio (CNR) were calculated. Contrast is computed as the normalized variation in the number of counts due the introduction of the absorption inhomogeneity and CNR indicates how this change in the number of counts compares with the overall fluctuations of the system. Contrast and CNR are computed as following:

$$C = \frac{N_0 - N}{N_0} \tag{2}$$

$$CNR = \frac{N_0 - N}{\sigma(N_0)} \tag{3}$$

where, N and N_0 are the inhomogeneous and homogeneous counts (i.e., with and without perturbation) and $\sigma(N_0)$ is the standard deviation of the homogeneous counts among the different repetitions.

It must be noted that to improve the depth sensitivity, contrast and CNR can be computed within well-defined portion of the DTOF defined with respect to the IRF peak position. The contrast and CNR were calculated for 7 different times gates of 1 ns width each. A more detailed explanation can be found in [15].

4) In Vivo Validation: In this case, several measurements were performed at various locations on a healthy subject to determine the maximum usable source-detector separation. The measurements were performed on following locations: 1) forehead, 2) parallel to inion and nasion, 3) diagonally along the head, 4) along the side of the chest, 5) diagonally along the chest, 6) on the belly, 7) on the thigh, 8) across the shoulder and 9) across the knee. Written informed consent was given by the subject and acquisitions were approved by the Ethical Committee of Politecnico di Milano and conducted in compliance with the Declaration of Helsinki.

The smallest source-detector separation was chosen as the distance at which the measured count-rate was around 2 Mcps. The source-detector separation was then increased by moving the source fiber at steps of 1 cm, until the count-rate dropped below 300 kcps. For each source-detector separation, 10 acquisitions of 1 s each were acquired. After each measurement on a different body location, IRF was acquired to fit the recorded DTOFs to retrieve the optical properties, as explained in Section II.B.2).

III. Results And Discussion

A. BIP Protocol

Fig. 3 shows the spectral responsivity of the 36 mm^2 area SiPM compared to cutting-edge research technology [5], state-of-the-art research technology [28] and state-of-the-art clinical technology [29]. The responsivity at 600 nm was measured to be 1×10^{-5} m^2sr and reduces to 1.83×10^{-7} m^2sr at 1000 nm due to the lower quantum efficiency of the detector. Responsivity value measured at a standard wavelength of 670 nm is the highest ever reported for SiPM detectors with a value of 7.54×10^{-6} m^2sr. As a comparison, the responsivity of the cutting-edge research technology that uses a 9 mm^2 area SiPM (with a fill-factor of 82%) directly in contact with the sample was measured to be 3.29×10^{-6} m^2sr thus improving the light harvesting capability by a factor of 2.28. The responsivity compared to state-of-the-art research and clinical technologies was found to be an order and two orders of magnitude higher respectively. The state-of-the-art research technologies employ 1×1 mm^2 area SiPM detectors placed in contact with the sample under measurement [28] whereas the research technology utilize hybrid Photomultiplier Tubes (PMTs) coupled using fiber bundles of 3 mm core diameter and an NA of 0.57 [29]. The improvement in the responsivity for the 36 mm^2 area SiPM can be ascribed to both the increase in the effective collection area as well as the large NA, as a result of the detector being placed in contact with the sample.

Fig. 4 shows IRF and its FWHM measured over a range of wavelengths from 600 nm to 1000 nm, in steps of 10 nm. As the injection wavelength increases, the IRF broadens, thus resulting in a larger FWHM (from 564.4 ps at 600 nm to 659.9 ps at 1000 nm). To compare, the FWHM of the cutting-edge research, state-of-the-art research and clinical system are 308 ps (at 670 nm), 215 ps (at 690 nm) and 450 ps (at 687 nm) respectively. Moreover, the IRF tail slope increases with wavelength while

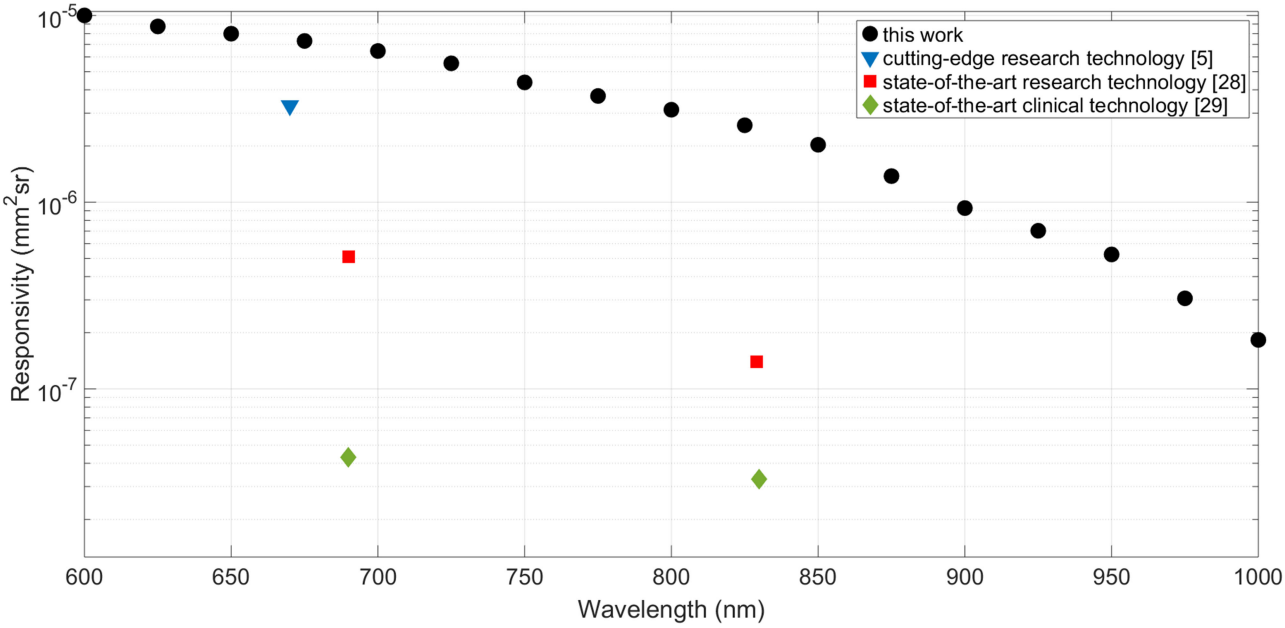

Fig. 3. Spectral responsivity compared with state-of-the art. The spectral trend in responsivity follows that of the photon detection efficiency of VUV Silicon, reducing by almost 2 orders of magnitude from 600 nm to 1000 nm.

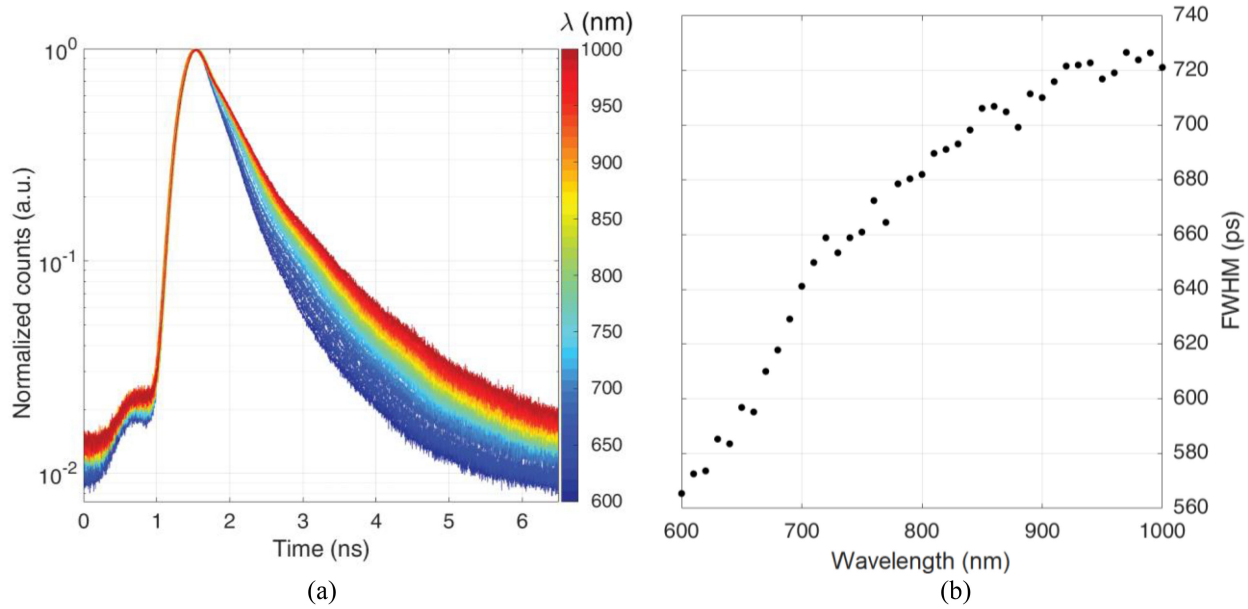

Fig. 4. (a) Spectral IRF normalized to peak spanning a spectral range from 600 nm (blue curve) to 1000 nm (red curve) in steps of 10 nm. (b) Variation of FWHM with injection wavelength.

the after-pulsing ratio, which is calculated as shown in (3), was found to be independent of the injection wavelength and remained constant at a value of 0.1904 ± 0.0055.

Fig. 5 shows the stability of i) total number of counts in the IRF, ii) its background noise floor, iii) FWHM and iv) barycenter temporal position. In each subplot of Fig. 5, the black dashed line represents the mean value over the whole 10 h interval after a 30-minute warm-up period and the red dotted lines represent the interval range of values around the average usually considered in diffuse optics applications. The fluctuations in the total number of counts and the background value were found to be well below ± 1% of the average value. Similarly, the variation in the FWHM and the barycenter of the IRF were found to be inside ± 10 ps of the mean value. Hence, the detector was found to be extremely stable over hours of operation without any significant drift, thus being in line with state-of-the-art devices [28], [29]. This was possible thanks to the TEC controller, which maintained the detector temperature at -15°C ± 1.5°C.

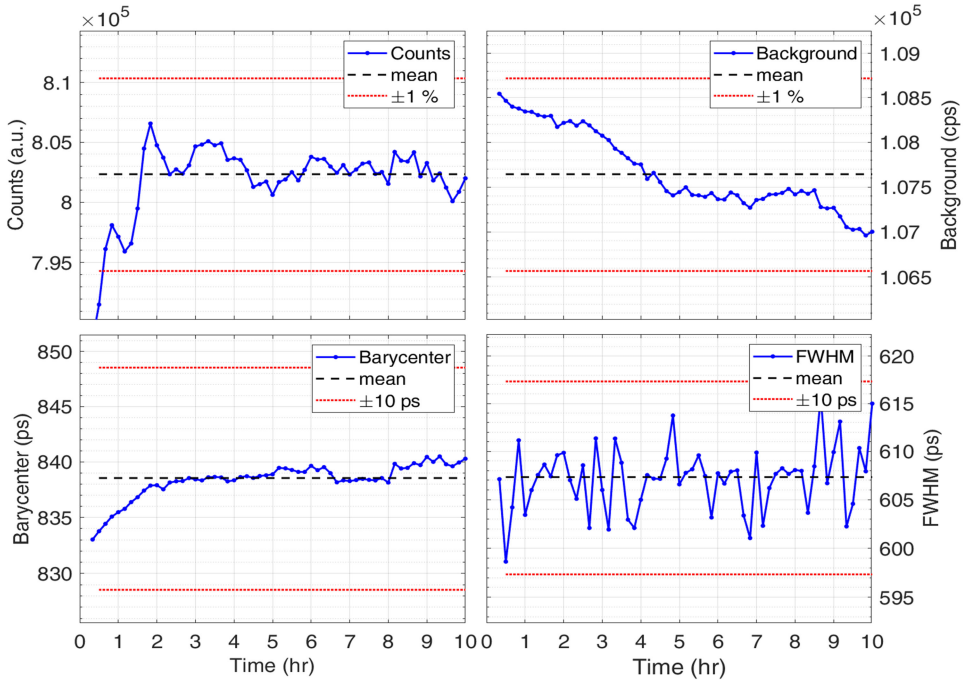

Fig. 5. Variation of total counts, background noise, FWHM of the IRF and the temporal position of its barycenter are plotted as blue curves with the dashed black line representing the average value over the entire interval after an initial warm-up period of 30 minutes. The red dotted lines represent the range of fluctuation usually considered ideal for the application in TD-DO.

B. MEDPHOT Protocol

Fig. 6 shows the results of the MEDPHOT protocol. Fig. 6 (a) shows the linearity plot of absorption. The dashed lines represent the trendlines calculated from the first 4 points (i.e., up to an absorption value of 0.21 cm^{-1}, which is considered as the typical range of optical properties for human tissue [29]). For $\mu_a \leq 0.21$ cm^{-1} the variation in the retrieved absorption is almost completely linear for all scattering values, while for larger absorption values, the retrieved absorption values deviate from linearity reaching a maximum deviation of 17%. The relative error in the retrieved μ_a is given by the accuracy and it was found to be 14.6% over the entire range and in the range corresponding to biological tissue (i.e., nominal $\mu_a \leq 0.21$ cm^{-1} nominal $\mu_s^{'}$<15 cm^{-1}), the accuracy improves to 8.5%. Fig. 6(b) shows the coupling between measured absorption and nominal scattering while in graph (c) the cross-talk between recovered scattering and conventionally true absorption is displayed. The retrieved values staying on an almost horizontal lines demonstrate that measured μ_a and $\mu_s^{'}$ are almost independent. There is a deviation for large absorption and scattering values due to the low number of counts which impair the fitting procedure. Finally, Fig. 6(d) shows retrieved scattering values plotted against nominal values. The linearity of the $\mu_s^{'}$ values is maintained for all absorption values with accuracy of 15.1% over the entire range and 5.9% in the range corresponding to biological tissues. The results obtained are in line with state-of-the-art systems capable of performing measurements in transmittance geometry. For instance, a 8 channel system based on SiPMs with active area of 1.3 × 1.3 mm^2 as described in [30], demonstrated very similar performance in terms of signal collection and reliable retrieval of optical properties of phantoms with high absorption and scattering properties (i.e., $\mu_a = 0.47$ cm^{-1} and $\mu_s^{'} = 20$ cm^{-1}). It must be noted that in that case the use of 8 SiPMs cooled results in a large optical responsivity while maintaining a low DCR at the expense of the system complexity: indeed, each SiPM has a signal output that has to be connected to a dedicated channel of the TDC. The current detector obtains the same performances with a single detector of active area 6 × 6 mm^2 with a higher responsivity, but also a much higher DCR.

C. nEUROPt Protocol

Figs. 7 and 8 show the measured Contrast and CNR respectively plotted at different penetration depths for various time gates (graphs). The contrast is plotted only for conditions (i.e., penetration depth and time window) corresponding to CNR > 1 (which is usually considered as the threshold for visibility of the perturbation). Once the CNR reaches the value of 1 (or lower), subsequent points are not considered and plotted in Fig. 7 since once the visibility threshold has been reached, if subsequent points featuring CNR > 1 they are not significant. As it is clear from Fig. 8, if the source-detector separation increases, the large responsivity of the detector enables the largest ever reported penetration depth of up to 40 mm, with a CNR > 1. Such a value is, to the best of our knowledge, the highest value reported in literature. Indeed, with an 8.6 mm^2 SiPM with tunable area and working in fast-gated mode (i.e., capable of enabling the detector in well-defined temporal window) the same perturbation was detected up to 37.5 mm [31].

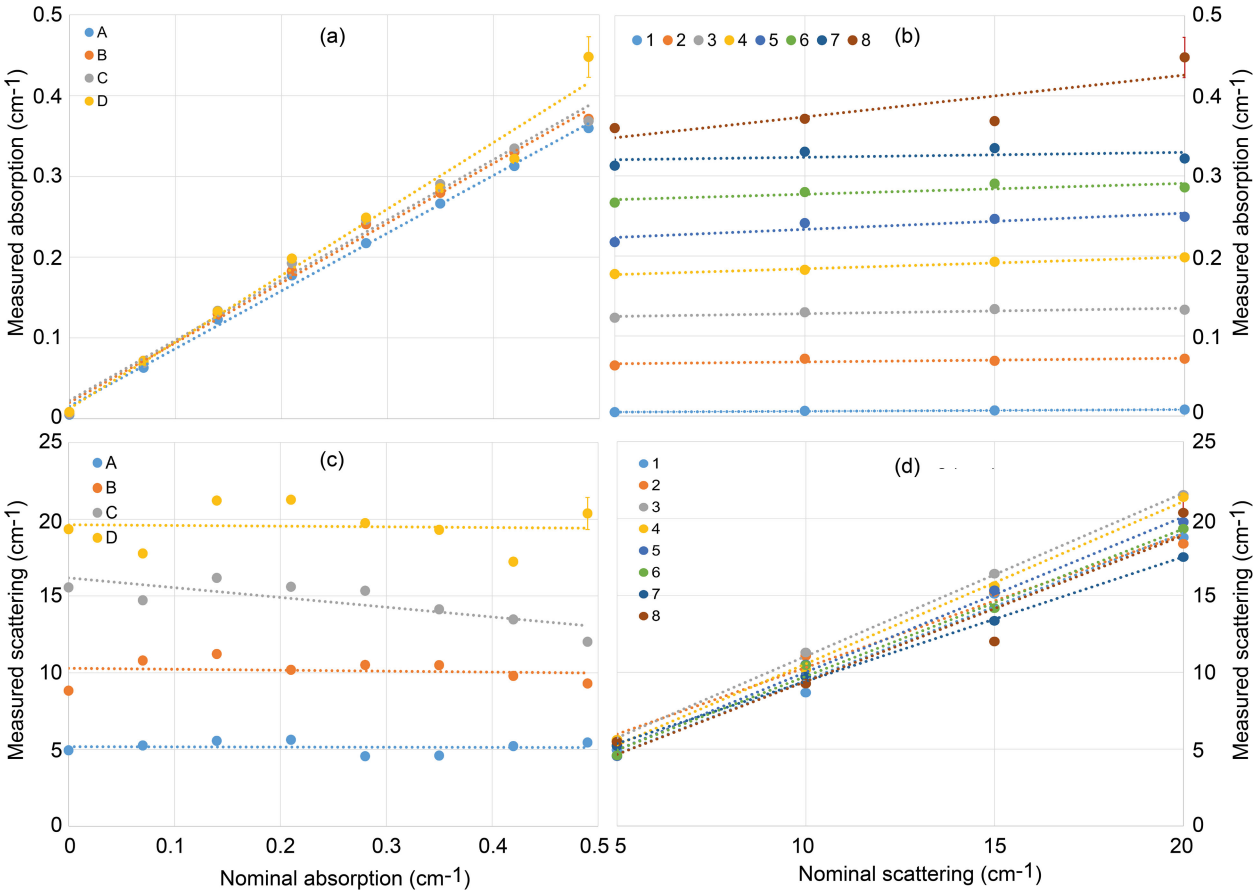

Fig. 6. Measured absorption and scattering coefficients (colored circles) plotted against nominal values. (a) shows the absorption linearity, (b) and (c) shows the coupling between retrieval of absorption and scattering coefficients and viceversa, (d) shows the linearity of scattering coefficients. Dotted lines represent the trendlines, while the error bars in all the plots (where visible exceeding the circles) correspond to standard deviation among 20 repetitions.

The high penetration depth opens up possibilities of measuring previously accessible regions of the brain such as the cerebellum as well as various internal organs like the heart or the lungs.

D. In Vivo Validation

In order to explore the usability of the current detector for *in-vivo* applications, various measurements were performed at multiple ρ. Fig. 9 shows the measured μ_a and μ_s' coefficients at different locations on the body, plotted against the source-detector separations. The error bars represent the standard deviation among the repetitions. The error bars are generally pretty small (maximum 20% of the average value) and are compatible with the biological variability. It must be noted that, for a given location, the error bars tend to increase upon an increase of the source-detector separation. Indeed, if the variable optical attenuator is fully open (i.e., all the laser power is shone on the skin) the increase in the ρ implies a decrease in the number of photons collected and in the dynamic range of the acquisition. Such a reduced dynamic range results in a more uncertain retrieval of the optical properties during fitting procedure, thus increasing the standard deviation. It must be noted that, even though large source-detector measurements up to 9 cm have been attempted before on phantoms and *in-vivo* [32], the setup was based on PMTs directly placed in contact with the sample/tissue. However, the use of SiPMs instead of PMTs permits easy scalability of the setup and increase the number of collection points (e.g., enabling the possibility to have tomographic images). Measurements on the forehead could be performed at a maximum source-detector separation of 10 cm. However, for belly a ρ of 16 cm has been reached. Looking at the graphs of Fig. 9, it is clear that the optical properties recovered for each location are not strongly dependent on the source-detector separation distance chosen for measurements. In our case, it has to be noted that the increase in the ρ performed by shifting the position of the source fiber implies probing slightly different regions of the body, as well as slightly changing the depth penetration. Thus, slight changes in the optical properties can be expected. Therefore, no strong conclusions can be drawn here. Our purpose was just to show the feasibility of in vivo measurements in this new regime, i.e., with the adoption for the first time to our knowledge of extremely large distances between source and detector points allowed by the high responsivity reported here.

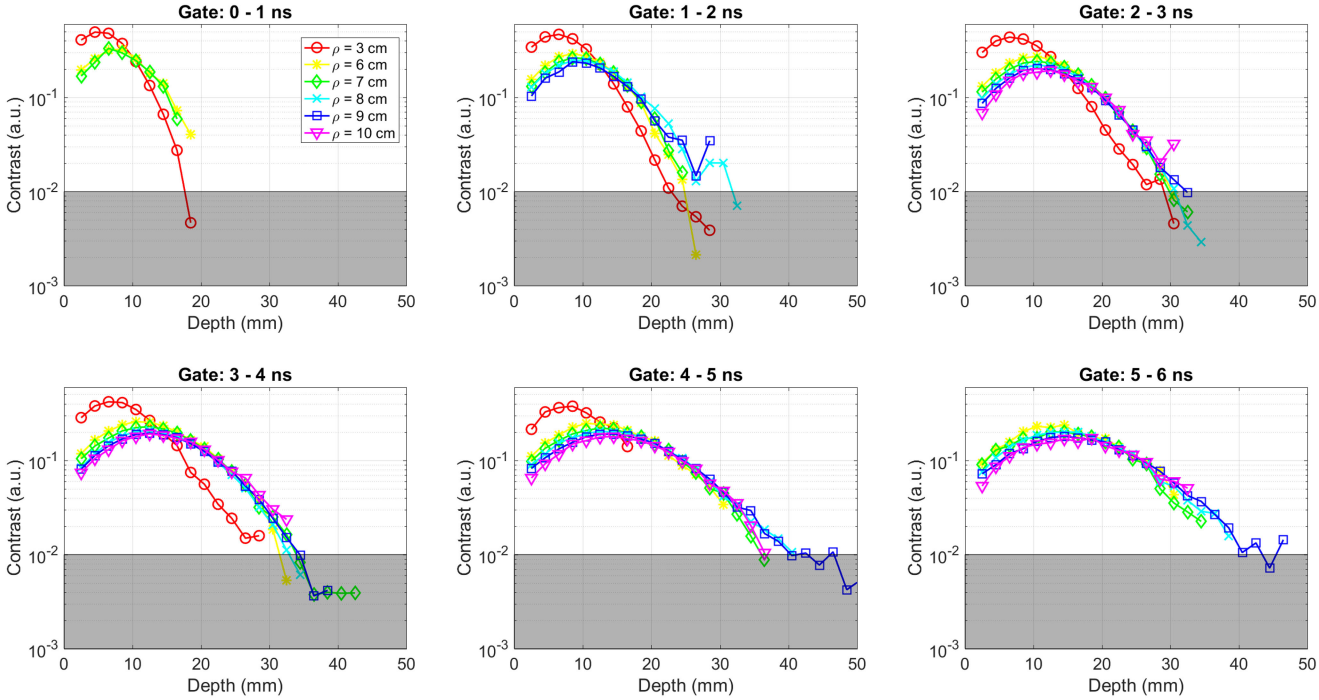

Fig. 7. Contrast computed for different time gates (graphs) using measurements at different ρ (colors). The gray shadow region indicates the range of values of biological fluctuations, thus where the contrast is too low to be distinguished.

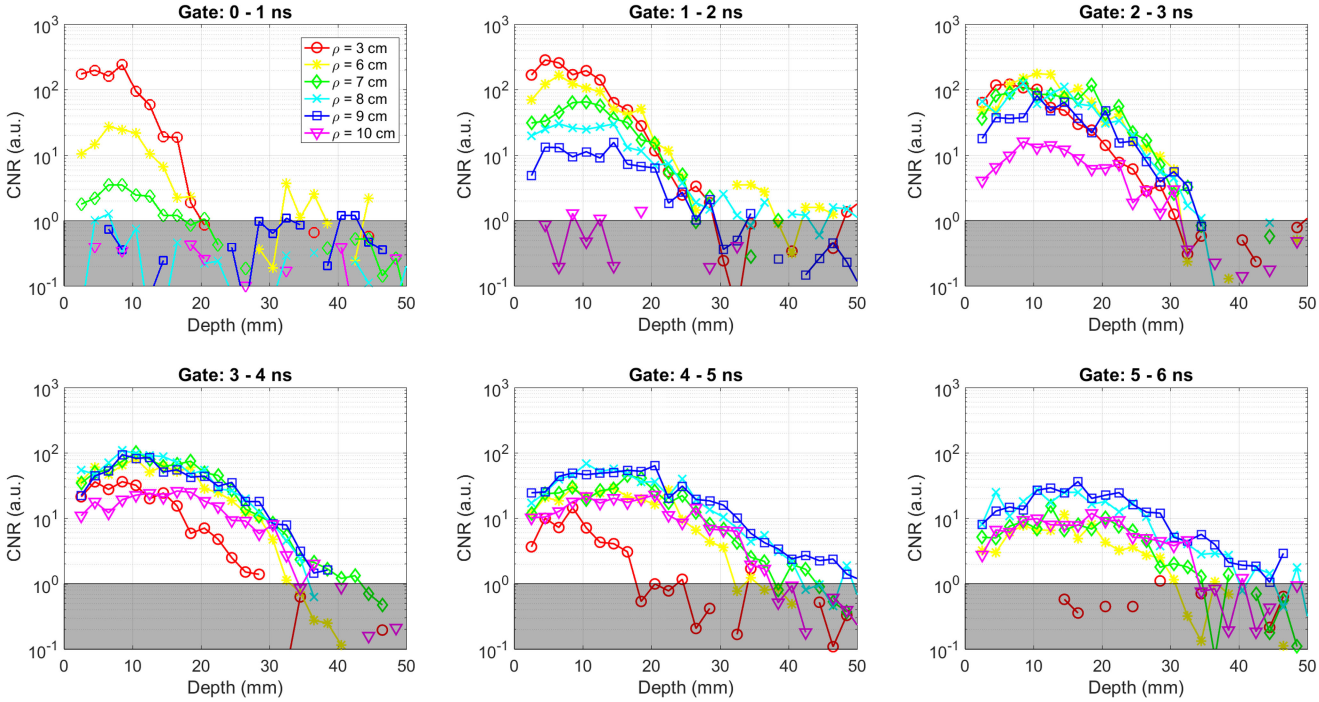

Fig. 8. CNR computed for different time gates (graphs) using measurements at different ρ (colors). The gray shadow region indicates the range where CNR < 1 (i.e., the theoretical threshold for perturbation visibility).

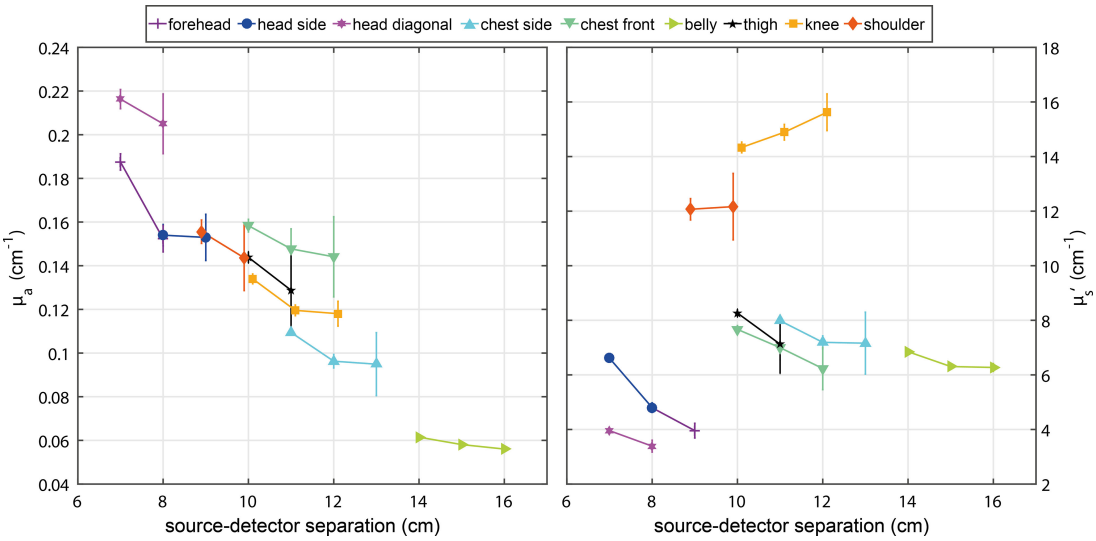

Fig. 9. Measured absorption and reduced scattering coefficient at various location on the body at multiple source-detector separations. The error bars represent the standard deviation among the repetitions.

IV. Conclusion

In this work we have demonstrated a novel large area SiPM detector, optimized for performance in TD-DO measurements with highest ever reported optical responsivity, moving closer to the goal of reaching the ultimate limit of performance. This device was validated under widely accepted standardized protocols, both at standard operating conditions as well as traditionally challenging conditions such as large source-detector distance and in transmittance geometry. The detector demonstrated good linearity and accuracy over the entire optical range. Moreover, even under challenging optical properties such as high absorption and low scattering, the values were retrieved with good accuracy. Additionally, a record penetration depth of 40 mm was achieved. This opens up new possibilities such as functional measurement on cerebellum and measurements on various internal organs, which were previously not possible.

Despite its impressive performance additional improvements are required to fully exploit the advantages offered by this technology. Even with a reduced background noise per mm^2 of active area, this still represents a limiting factor since it limits the overall dynamic range offered by this detector.

Possible steps in this field will include integration of a high throughput timing electronics to maximize the number of detected counts thereby hugely improving the signal-to-noise ratio as well as the depth penetration [5]. The eventual goal of a detector with low noise (1-2 Mcps per 1 cm^2), good timing resolution and a collection area of 1 cm^2, will require exploitation of innovative layouts as well as further segmentation of the active area. This detector can form a key component of a low-cost optical probe that can be embedded in clinical and preclinical devices for continuous, non-invasive monitoring of patients' health. The possibility of performing measurements in transmittance geometry opens new and exciting possibilities of cerebral monitoring and monitoring major organs in transmittance geometry.

References

[1] S. L. Jacques, "Time-resolved reflectance spectroscopy in turbid tissues," *IEEE Trans. Biomed. Eng.*, vol. 36, no. 12, pp. 1155–1161, Dec. 1989.

[2] A. Pifferi *et al.*, "New frontiers in time-domain diffuse optics, a review," *J. Biomed. Opt.*, vol. 21, no. 9, 2016, Art. no. 091310.

[3] A. Dall. Mora *et al.*, "The SiPM revolution in time-domain diffuse optics," *Nucl. Instruments Methods Phys. Res. Sect. A Accel. Spectrometers, Detect. Assoc. Equip.*, vol. 978, 2020, Art. no. 164411.

[4] S. Fujisaka *et al.*, "A clinical tissue oximeter using NIR time-resolved spectroscopy," in *Oxygen Transport to Tissue XXXVII*, 2016, pp. 427–433.

[5] L. Di Sieno *et al.*, "Probe-hosted large area silicon photomultiplier and high-throughput timing electronics for enhanced performance time-domain functional near-infrared spectroscopy," *Biomed. Opt. Exp.*, vol. 11, no. 11, 2020, Art. no. 6389.

[6] H. Y. Ban *et al.*, "Kernel flow: A high channel count scalable TD-fNIRS system," *Integr. Sensors for Biol. Neural Sens.*, vol. 11663, pp. 24–42, 2021.

[7] C. Niclass, C. Favi, T. Kluter, M. Gersbach, and E. Charbon, "A 128 × 128 single-photon image sensor with column-level 10-bit time-to-digital converter array," *IEEE J. Solid-State Circuits*, vol. 43, no. 12, pp. 2977–2989, Dec. 2008.

[8] C. Niclass, M. Soga, H. Matsubara, and S. Kato, "A 100m-range 10-frame/s 340x96-pixel time-of-flight depth sensor in 0.18μm CMOS," in *Proc. Eur. Solid-State Circuits Conf.*, 2011, pp. 107–110.

[9] D. Tyndall *et al.*, "A high-throughput time-resolved mini-silicon photomultiplier with embedded fluorescence lifetime estimation in 0.13 μm CMOS," *IEEE Trans. Biomed. Circuits Syst.*, vol. 6, no. 6, pp. 562–570, Dec. 2012.

[10] N. A. W. Dutton *et al.*, "1.5 A time-correlated single-photon-counting sensor with 14GS/S histogramming time-to-digital converter," in *Proc. Dig. Tech. Pap. - IEEE Int. Solid-State Circuits Conf.*, San Francisco, CA, USA, 2015, pp. 204–205.

[11] N. Krstajić *et al.*, "05 billion events per second time correlated single photon counting using CMOS SPAD arrays," *Opt. Lett.*, vol. 40, no. 18, 2015, Art. no. 4305.

[12] P. GmbH, "MultiHarp 150." Accessed: Mar. 2, 2020. [Online]. Available: https://www.picoquant.com/products/category/tcspc-and-time-tagging-modules/multiharp-150-high-throughput-multichannel-event-timer-tcspc-unit#specification

[13] H. Wabnitz *et al.*, "Performance assessment of time-domain optical brain imagers, Part 1: Basic instrumental performance protocol," *J. Biomed. Opt.*, vol. 19, no. 8, 2014, Art. no. 86010.

[14] A. Pifferi *et al.*, "Performance assessment of photon migration instruments: The MEDPHOT protocol," *Appl. Opt.*, vol. 44, no. 11, pp. 2104–2114, Apr. 2005.

[15] H. Wabnitz *et al.*, "Performance assessment of time-domain optical brain imagers, Part 2: NEUROPt protocol," *J. Biomed. Opt.*, vol. 19, no. 8, 2014, Art. no. 86012.

[16] F. Acerbi *et al.*, "Silicon photomultipliers: Technology optimizations for ultraviolet, visible and near-infrared range," *Instruments*, 2019.

[17] A. Jamil *et al.*, "VUV-Sensitive silicon photomultipliers for Xenon scintillation light detection in nEXO," *IEEE Trans. Nucl. Sci.*, vol. 65, no. 11, pp. 2823–2833, Nov. 2018.

[18] C. Rethmeier, "Characterization of VUV sensitive SIPMS for nEXO," *Journal of Instrumentation*, 2016.

[19] M. Capasso *et al.*, "FBK VUV-sensitive silicon photomultipliers for cryogenic temperatures," *Nucl. Instruments Methods Phys. Res. Sect. A Accel. Spectrometers, Detect. Assoc. Equip.*, 2020.

[20] F. Acerbi, A. Behera, A. Dalla Mora, L. Di Sieno, and A. Gola, "Single-photon detection module based on large-area silicon photomultipliers for time-domain diffuse optics," *Instruments*, vol. 5, no. 2, 2021.

[21] M. Firbank, M. Oda, and D. T. Delpy, "An improved design for a stable and reproducible phantom material for use in near-infrared spectroscopy and imaging," *Phys. Med. Biol.*, vol. 40, no. 5, 1995, Art. no. 955.

[22] D. Contini, F. Martelli, and G. Zaccanti, "Photon migration through a turbid slab described by a model based on diffusion approximation i theory," *Appl. Opt.*, 1997.

[23] F. Martelli, D. Contini, A. Taddeucci, and G. Zaccanti, "Photon migration through a turbid slab described by a model based on diffusion approximation. II. Comparison with Monte Carlo results," *Appl. Opt.*, vol. 36, no. 19, pp. 4600–4612, 1997.

[24] R. C. Haskell *et al.*, "Boundary conditions for the diffusion equation in radiative transfer," *JOSA A*, vol. 11, no. 10, pp. 2727–2741, 1994.

[25] F. Martelli *et al.*, "Phantoms for diffuse optical imaging based on totally absorbing objects, Part 1: Basic concepts.," *J. Biomed. Opt.*, vol. 18, no. 6, Jan. 2013, Art. no. 066014.

[26] F. Martelli *et al.*, "Phantoms for diffuse optical imaging based on totally absorbing objects, Part 2: Experimental implementation," *J. Biomed. Opt.*, vol. 19, no. 7, 2014, Art. no. 76011.

[27] L. Spinelli *et al.*, "Determination of reference values for optical properties of liquid phantoms based on intralipid and India ink," *Biomed. Opt. Exp.*, vol. 5, no. 7, pp. 2037–2053, 2014.

[28] R. Re *et al.*, "Probe-hosted silicon photomultipliers for time-domain functional near-infrared spectroscopy: Phantom and in vivo tests," *Neurophotonics*, vol. 3, no. 4, 2016, Art. no. 045004.

[29] R. Re *et al.*, "Multi-channel medical device for time domain functional near infrared spectroscopy based on wavelength space multiplexing," *Biomed. Opt. Exp.*, vol. 4, no. 10, pp. 2231–2246, 2013.

[30] E. Ferocino *et al.*, "High throughput detection chain for time domain optical mammography," *Biomed. Opt. Exp.*, vol. 9, no. 2, pp. 755–770, 2018.

[31] L. Di Sieno *et al.*, "Probe-hosted large area silicon photomultiplier and high-throughput timing electronics for enhanced performance time-domain functional near-infrared spectroscopy," *Biomed. Opt. Exp.*, vol. 11, no. 11, pp. 6389–6412, Nov. 2020.

[32] A. Liebert *et al.*, "Assessment of inflow and washout of indocyanine green in the adult human brain by monitoring of diffuse reflectance at large source-detector separation," *J. Biomed. Opt.*, vol. 16, no. 4, pp. 46011–46017, 2011.

Anurag Behera was born in Orissa, India, in 1994. He received the master's degree in physics with a specialization in photonics from SSSIHL, India, in 2016 and the Ph.D. degree in physics from Politecnico di Milano, Milan, Italy, in 2020 under the Marie Skłodowska-Curie Actions fellowship. He is currently a Postdoctoral Researcher with The Institute of Photonic Sciences (ICFO), Barcelona, Spain. Dr. Behera's current research interests include high-density hybrid diffuse optic devices, with an emphasis on translational research.

Fabio Acerbi (Member, IEEE) was born in Carpi, Italy, in 1984. He received the bachelor's degree in electronics engineering from the University of Modena and Reggio Emilia, Modena, Italy, in 2006, the master's degree from the Politecnico di Milano, Milan, Italy, in 2008 (both *summa cum laude*), where he received the Ph.D. degree in information technology in 2012. From 2009 to 2013, he was with the Department of Electronics, Information and Bioengineering (DEIB) of the Politecnico di Milano, where he worked on InGaAs/InP single-photon avalanche diodes (SPADs). Since 2013, he has been working with Fondazione Bruno Kessler (FBK), Trento, Italy, on the design and development of Silicon Photomultipliers (SiPM), SPAD, readout electronics, radiation effects in silicon detectors, quantum random number generators, and pinned photodiode imagers.

Alberto Gola was born in Milano, Italy, in 1978. He received the five-years degree in electronic engineering in 2003 and the Ph.D. degree in information technology engineering in 2007 from the Politecnico of Milano, Italy. From 2007 to 2009, he was with the Department of Electronic Engineering of the Politecnico di Milano in a Postdoc position. His research interests include Silicon Drift Detectors, SDD-based Gamma Cameras, multi-channel ASIC design, DAQ systems, optimal filtering and signal processing. Since 2010, he has been with Fondazione Bruno Kessler, Trento, Italy, as a Junior Researcher focusing on the development of Silicon Photomultipliers and the related readout electronics.

Alberto Dalla Mora was born in Fiorenzuola d'Arda, Italy, in 1981. He received the M.S. degree in electronics engineering and the Ph.D. degree in information and communication technology from Politecnico di Milano, Italy, in 2006 and 2010, respectively. He is currently an Associate Professor with the Physics Department of Politecnico di Milano, Italy. He has authored about 170 papers in international peer-reviewed journals and conference proceedings. Prof. Dalla Mora's research interests mainly include the development of innovative time-resolved diffuse optics techniques and instrumentation for biomedical applications.

Laura Di Sieno was born in Varese, Italy, in 1987. She received the master's degree in electronics engineering and the Ph.D. degree in physics from the Politecnico di Milano, Milan, Italy, in 2011 and 2015, respectively. She is currently an Assistant Professor with the Department of Physics, Politecnico di Milano. She has authored more than 80 papers in international peer-reviewed journals and conference proceedings. Dr. Di Sieno's activity is mainly focused on the study and application of a new approach and instrumentation for time-domain optical spectroscopy of highly scattering media using single-photon detectors.